The molecular electrometer and binding of cations to phospholipid bilayers

Andrea Catte,[*] Mykhailo Girych,[†] Matti Javanainen,[‡] Claire Loison, Josef Melcr,[§] Markus S. Miettinen,[¶] Luca Monticelli,[**] Jukka Määttä,[††] Vasily S. Oganesyan,[*] O. H. Samuli Ollila,[‡‡] Joona Tynkkynen,[‡] and Sergey Vilov

Despite the vast amount of experimental and theoretical studies, the binding affinity of cations, especially the biologically relevant Na^+ and Ca^{2+} ions, into a phosholipid bilayer is not agreed on in the literature. Here we show that the ion binding affinity can be directly compared between simulations and experiments by using the choline headgroup order parameters according to the 'molecular electrometer' concept. [1].

Our results strongly support the traditional view that Na^+ ions and other monovalent ions (bar Li^+) do not specifically bind to phosphatidylcholine lipid bilayers with mM concentrations, in contrast to Ca^{2+} and other multivalent ions. Especially the Na^+ binding affinity is overestimated by several molecular dynamics simulation models, leading to an artificially positively charged lipid bilayer. Qualitatively correct headgroup order parameter response is observed with Ca^{2+} binding in all the tested models, however, none of the tested models has sufficient quantitative accuracy to interpret the Ca^{2+}:lipid stoichiometry or the induced atomistic resolution structural changes.

This work has been, and continues to be, progressed and discussed through the blog `nmrlipids.blogspot.fi`*, through which everyone is invited to join the discussion and make contributions. The manuscript will be eventually submitted to an appropriate scientific journal. Everyone who has contributed to the work through the blog will be offered coauthorship. For more details see* `nmrlipids.blogspot.fi`*.*

I. INTRODUCTION

The interaction of cations with phospholipid membranes is important in many physiological processes, nerve cell signalling being the prime example. For this reason such interactions have been widely studied via experiments, simulations, and theory. While it is generally agreed that the relative binding affinity of different ions follows the Hofmeister series [2–10], no consensus emerges from the literature on the quantitative binding affinities of different ions to phospholipid bilayers. Two extensive reviews covering work done prior to 1990 [3, 4] concluded that monovalent cations interact only weakly with phospholipid bilayers (with the exception of Li^+), while for multivalent ions the interactions are significant. This conclusion has been supported by further studies showing that bilayer properties remain unaltered upon addition of millimolar concentrations of monovalent salt [5, 11, 12]. On the other hand, the weakness of interactions between phospholipids and monovalent ions has been questioned in several experimental and molecular dynamics simulation studies [7–10, 13–19] suggesting stronger binding especially for Na^+ ions.

More specifically, millimolar concentrations of NaCl have a negligible effect on the choline head group order parameters [20], area per molecule [11], dipole potential [21], and lipid lateral diffusion [12]; in contrast, these properties are significantly affected by the presence of $CaCl_2$ or other multivalent ions. In addition, water sorption isotherms are very similar for POPC/NaCl system and NaCl in pure water — indicating only weak interaction between ion and lipids [5]. Further, only minor changes in POPC infrared spectra are observed in the presence of NaCl, while changes are significant in the presence of Ca^{2+} and other multivalent ions, also confirming that interaction between Na^+ and lipids are weak [5]. In contrast, the decrease in rotational and translational dynamics of fluorescent probes in lipid bilayers with mM NaCl concentrations suggests significant Na^+ binding [8, 10, 13]. However, the reduced lateral diffusion is not observed in non-invasive NMR experiments, suggesting that fluorescence results arise from Na^+ interactions with probes rather than with lipids [12]. Also the interpretation of calorimetric measurements has been controversial. The effect of monovalent ions (bar Li^+) on phase transition temperature is small, compared to the effect of multivalent ions; this was initially interpreted by Cevc as an indication that only multivalent ions and Li^+ specifically bind to phosholipid bilayers [3]; however, more recently such small effect was interpreted as an indication that also Na^+ binds to lipid membranes [9, 13]. In electrophoresis measurements on phosphatidylcholine vesicles, NaCl increases the (initially negative) zeta potential to about zero; however, positive zeta potentials can be generally reached only with multivalent ions or Li^+ [2, 9, 15, 16, 22]. The lack of significant positive electrophoretic mobility in the presence of NaCl suggests weak binding of Na^+; however, the same data can also be explained by the effect of Cl^- ions [23, 24].

[*] University of East Anglia, Norwich, United Kingdom
[†] Helsinki Biophysics and Biomembrane Group, Department of Biomedical Engineering and Computational Science, Aalto University, Espoo, Finland
[‡] Tampere University of Technology, Tampere, Finland
[§] Institute of Organic Chemistry and Biochemistry, Czech Academy of Sciences, Flemingovo nam. 2, 16610 Prague 6, Czech Republic, Charles University in Prague, Faculty of Mathematics and Physics, Ke Karlovu 3, 121 16 Prague 2, Czech Republic
[¶] Fachbereich Physik, Freie Universität Berlin, Berlin, Germany
[**] Institut de Biologie et Chimie des Protéines (IBCP), CNRS UMR 5086, Lyon, France
[††] Aalto University, Espoo, Finland
[‡‡] **Author to whom correspondence may be addressed. E-mail: samuli.ollila@aalto.fi.**,Department of Neuroscience and Biomedical Engineering, Aalto University, Espoo, Finland

Finally, changes in bilayer hardness and area per lipid measured with Atomistic Force Microscopy (AFM) were interpreted as Na^+ binding to phospholipids [15–19].

Atomistic molecular dynamics (MD) simulations are a powerful tool to interpret experimental data in terms of atomic-level interactions. In atomistic MD simulations, the majority of commonly used models predicts binding of Na^+ ions to phoshatidylcholine lipid bilayers, but the strength of binding depends on the specific model used [13, 14, 23, 25–29]. Some simulation studies confirmed a reduction in lipid lateral diffusion due to Na^+ binding, in agreement with fluorescent probe measurements [8, 10, 13] but in contrast with NMR experiments [12]. Other simulations showed a reduction in area per lipid in the presence of NaCl, in agreement with AFM experiments [15–19]; however, the reduction in area was observed at excessively low Na^+ concentrations, compared to observations from scattering experiments [11]. Predictions of electrophoretic mobility in the presence of NaCl yielded positive values, higher than in experiments; however, this could be explained by the behaviour of Cl^- ions [23, 24].

In the present work we set out to solve the apparent contradictions by directly comparing the headgroup hydrocarbon segment α and β (see Fig. 1) order parameters between simulations and experiments as a function of cation concentration. According to the 'molecular electrometer' concept, changes in order parameters of the α and β carbons in the phospholipid head group can be used to measure the ion affinity to the phophatidylcholine (PC) lipid bilayer [1, 20, 30, 31]. Order parameters can be accurately measured in experiments and straightforwardly compared to simulations [32], therefore the molecular electrometer allows the comparison of binding affinity between simulations and experiments. We show that the response of order parameters to penetrating cations is qualitatively correct in simulations, but the affinity of PC bilayers for Na^+ ions is significantly overestimated in several MD simulation models. Moreover, we show that the accuracy of tested models does not allow for an interpretation of lipid–Ca^{2+} interactions with atomistic resolution.

II. RESULTS AND DISCUSSION

A. Molecular electrometer concept in experiments

According to the molecular electrometer concept the binding of charged objects on PC bilayer interface induce systematic changes in choline β and α segment order parameters. Thus, the changes of these order parameters can be used to determine binding affinities of the charged objects. The concept is originally based on experimentally observed changes in choline order parameters with bound cations [20, 30], see Fig. 2 for data as a function of ion concentration in solution.

Further quantification with various positively and negatively charged molecules showed that choline order parameters vary linearly with small amount of bound charge per lipid [1, 30, 31, 37–42]. The relation between bound charge per lipid $X^{\pm}$ and choline order parameters can be then written as [**?**]

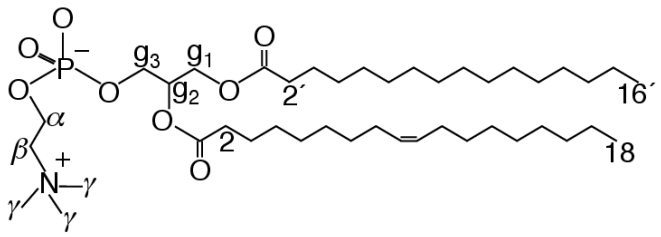

FIG. 1: Chemical structure of 1-palmitoyl-2-oleoylphosphatidylcholine (POPC).

$$S^i_{\rm CH}(X^{\pm}) = S^i_{\rm CH}(0) + \frac{4}{3}\chi^{-1} m_i X^{\pm}, \qquad (1)$$

where the quadrupole coupling constant χ is approximately equal to 167 kHz, $S^i_{\rm CH}(0)$ is order parameter without bound charges, m_i is constant depending on the valency and position of bound charge, and i refers to either α or β. The order parameter change respect to a bilayer without bound charges then becomes

$$\Delta S^i_{\rm CH} = S^i_{\rm CH}(X^{\pm}) - S^i_{\rm CH}(0) = \frac{4}{3}\chi^{-1} m_i X^{\pm}. \qquad (2)$$

Combination of atomic absorption spectra and ^{2}H NMR experiments gave $m_\alpha = -20.5$ and $m_\beta = -10.0$ for Ca^{2+} binding in POPC bilayer in the presense of 100mM NaCl [30].

The quantification of β and α segment order parameter changes with different cations have revealed that $\Delta S^\beta_{\rm CH}/\Delta S^\alpha_{\rm CH} \approx 0.5$ for wide range of different cations (aqueous cations, cationic peptides, cationic anesthetics) [40, 42]. More specifically, the experimental data shown in Fig. 3 led to the relation $\Delta S^\beta_{\rm CH} = 0.43\Delta S^\alpha_{\rm CH}$ for DPPC bilayer with various $CaCl_2$ concentrations [20].

In original experiments the absolute values of order parameters increased for β and decreased for α segment with bound positive charge and *vice versa* for negative charge [1, 20, 30, 31, 37, 42]. However, more recent experiments showed that β carbon order parameter is negative while α carbon order parameter is positive [33–35]. Thus, we can conclude that β and α segment order parameters decrease with bound positive charges and increase with bound negative charge. Consequently, values of m_i are negative for bound positive charges and *vice versa*. This can be rationalized by electrostatically induced changes in choline P-N dipole tilt [1, 31, 43] which is also seen in simulations [26, 27, 44]. This is in line with order parameter decrease related to the P-N vector tilting more

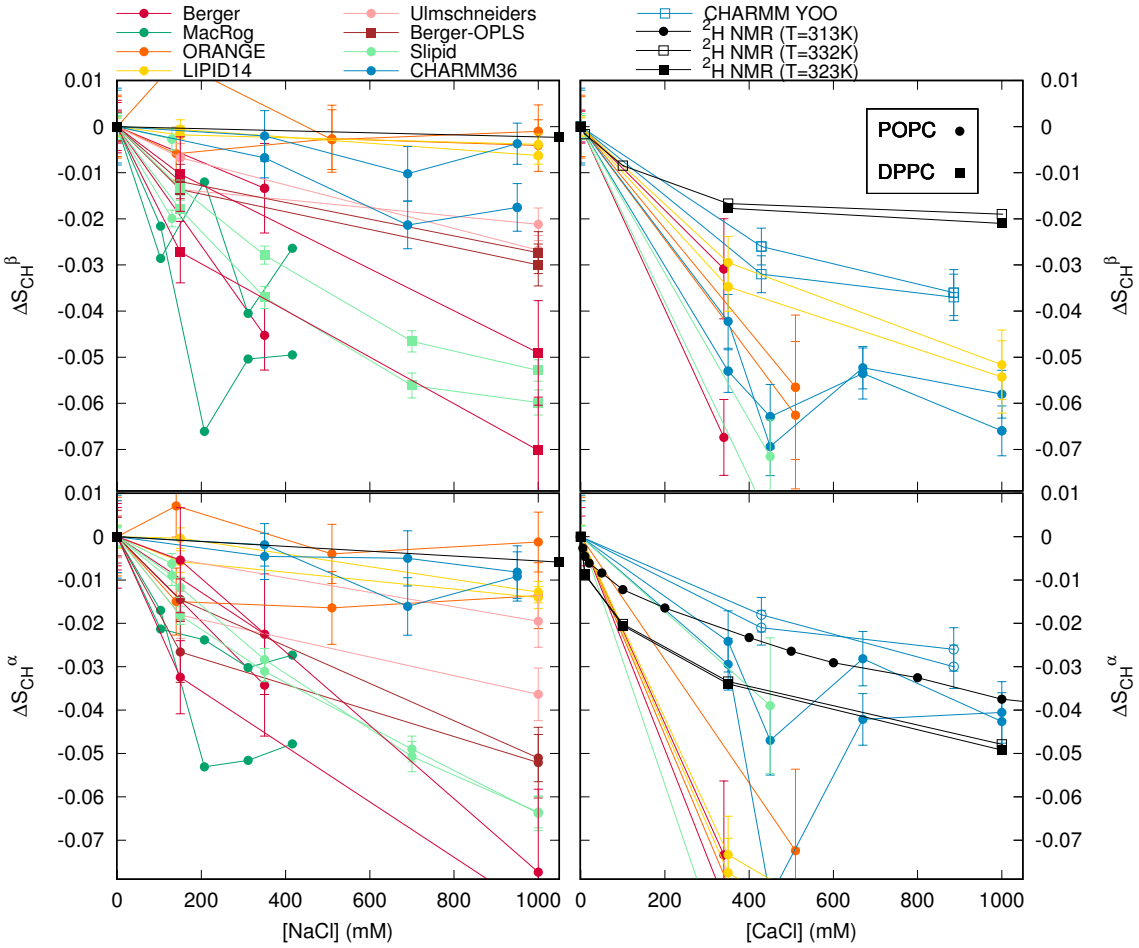

FIG. 2: The order parameter changes for β and α segments as a function of NaCl (left column) and $CaCl_2$ (right column) concentration, from simulations and experiments [20] (POPC with $CaCl_2$ from [30]). The signs of the experimental order parameters, taken from experiments without ions [33–35], can be assumed to be unchanged with concentrations represented here [30, 32]. It should be noted that none of the models used here reproduces the order parameters within experimental error for pure PC bilayer without ions, indicating structural inaccuracies with varying severity in all models [36]. Note that the relatively large decrease in CHARMM36 with 450 mM $CaCl_2$ arise from more equilibrated binding affinity due to long simulation times, see supplementary information.

1.DONE

parallel to membrane plane seen with decreased hydration levels [36].

The headgroup order parameter changes as a function of ion concentration in solution from H^2 NMR experiments are shown in Fig. 2 for DPPC and POPC bilayers [20, 30]. In contrast to the response as a function of bound charge in Eq. 1, the changes in Fig. 2 are not linear. This can be explained by electrostatic repulsion between already bound Calcium ions and ions in solution [30]. Experimental data in Fig. 2 shows only minor changes in order parameter as a function of NaCl is solution, while the effect of $CaCl_2$ is an order of magnitude larger. Thus, according to the molecular electrometer concept, monovalent Na^+ ions have negligible affinity for PC lipid bilayers at concentrations up to 1 M, while binding of Ca^{2+} ions at the same concentration is significant [20, 30]. This conclusion is in agreement with several other experimental studies [3–5, 11, 12].

B. Molecular electrometer concept in MD simulations

Figure 2 also reports order parameter changes calculated from MD simulations of DPPC and POPC lipid bilayers as a function of NaCl or $CaCl_2$ concentrations in solution. Details of the simulated systems are reported in Table I and in Supplementary Information. It should be noted that none of the models used here reproduced the order parameters for pure PC bilayer without ions within experimental uncertainty in our previous study (Figure 2 in Ref. [36]), indicating structural inaccuracies with varying severity for all models [36]. On the other hand, the experimentally observed headgroup order parameter increase with dehydration was qualitatively reproduced by all the tested models [36]. Accordingly, the presense of cations in simulations leads to the decrease of choline order parameters in Fig. 2, which is in qualitative agreement with experiments. However, the changes are overestimated in most

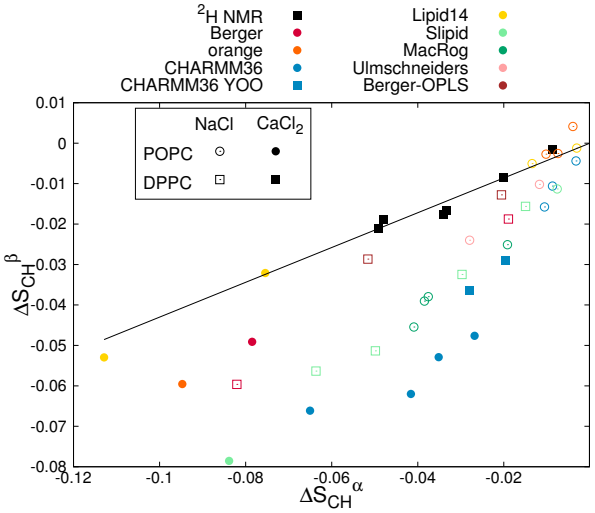

FIG. 3: Relation between $\Delta S^{\beta}_{\mathrm{CH}}$ and $\Delta S^{\alpha}_{\mathrm{CH}}$ from experiments [20] and different simulation models. Solid line is $\Delta S^{\beta}_{\mathrm{CH}} = 0.43 \Delta S^{\alpha}_{\mathrm{CH}}$ determined for DPPC bilayer from ^{2}H NMR experiment with various $CaCl_2$ concentrations [20].

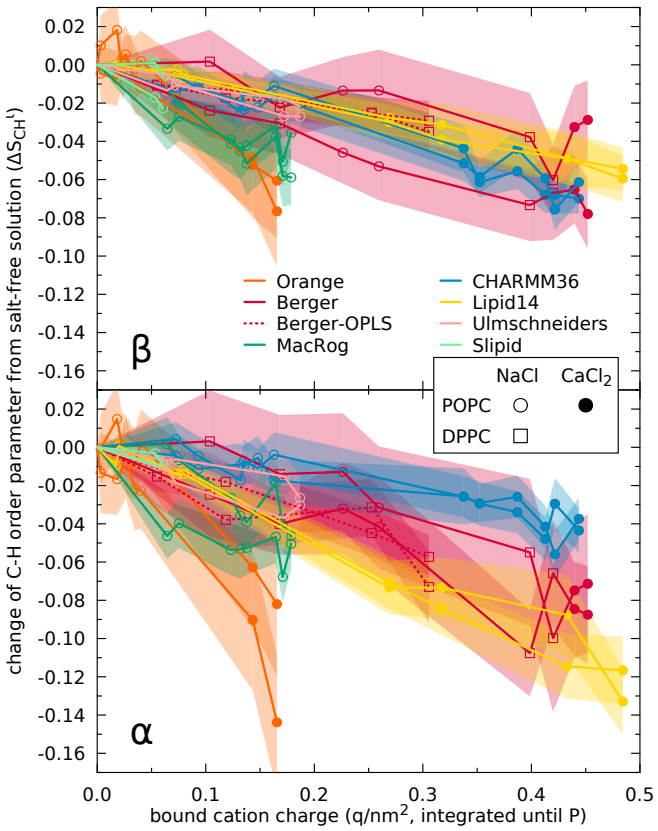

FIG. 4: Order parameters changes $\Delta S^{\beta}_{\mathrm{CH}}$ and $\Delta S^{\alpha}_{\mathrm{CH}}$ as a function of bound cations from different simulation models.

2.Results from long CHARMM and Slipids simulations to be added. Description of the calculation of bound charges to be described, probably in supplementary.

simulation results in Fig 2.

According to the electrometer concept the order parameter changes are proportional to the amount of bound cations in bilayer, see Eq. 2. The order parameter changes as a function of bound charge from simulations are shown in Fig. 4. Roughly linear correlation between bound charge and order parameter change is found in all simulation models, which is in line with experiments [30]. However, there are some differences in the proportionality constans (i.e. slopes in Fig. 4) between different models; especially MacRog and Orange models give relatively steep slopes and CHARMM gives gentle slope for α carbon. The quantitative comparison to experimental slopes ($m_\alpha = -20.5$ and $m_\beta = -10.0$ for Ca^{2+} binding in DPPC bilayer in the presense of 100mM NaCl in Eq. 1 [30]) is not straightforward since the simulation results depend on the definition used for bound ions.

The comparison of order parameter changes as a function of bound charge is more straightforward for systems with charged amphihiles, which are fully associated in bilayer. In this case the amount of bound charge is explicitly known in both, simulations and experiment. Such comparison is done between previously published simulation data [45] and experiments [31, 46] in Supplementary Information. The overestimation of order parameter response to bound cations (i.e. slopes m_β and m_α) could not be ruled out in the Berger based model. In principle, this might explain the overestimated order parameter response to $CaCl_2$ with Berger model, but not overestimated response to NaCl (see discussion in Supplementary Information). The more detailed comparison with different models is left for further studies.

The relation between $\Delta S^{\beta}_{\mathrm{CH}}$ and $\Delta S^{\alpha}_{\mathrm{CH}}$ from different simulation models is compared to experiments in Fig. 3. Almost all the tested models give larger $\Delta S^{\beta}_{\mathrm{CH}}/\Delta S^{\alpha}_{\mathrm{CH}}$ ratio than in experiments [20]; only Lipid14 give values in agreement with experimental ratio. Thus, in all the other tested simulation models α order parameter decrease is underestimated in respect to β order parameter decrease with bound cations.

Figure 4 shows that order parameter decrease clearly correlates with the amount of bound cations also in simulations. This is also evident from Fig. 5 showing Na^+ density profiles from the different simulation models. In the figure, simulation models are ordered according to the order parameter changes (reported Fig. 2), from the smallest to the largest. The Na^+ density peaks are larger for models with larger changes in order parameters, in line with observed correlation between cation binding and order parameter decrease in Fig. 4.

In conclusion, the clear correlation between bound cations and order parameter decrease is observed in all the tested simulation models. However, quantitative responses of α and β on bound cations do not generally agree with experiments because the $\Delta S^{\beta}_{\mathrm{CH}}/\Delta S^{\alpha}_{\mathrm{CH}}$ ratio agrees with experiments only in Lipid14 model (Fig. 3). Thus, the observed overestimations of order parameter changes with cation concentrations may, in principle, arise from overbinding of ions or from too sensitive lipid headgroup response on bound cation (see also discussion in Supplementary Material). Consequently, the electrometer concept can be used to quantitatively compare the cation binding affinity between experiments and simulations, but careful

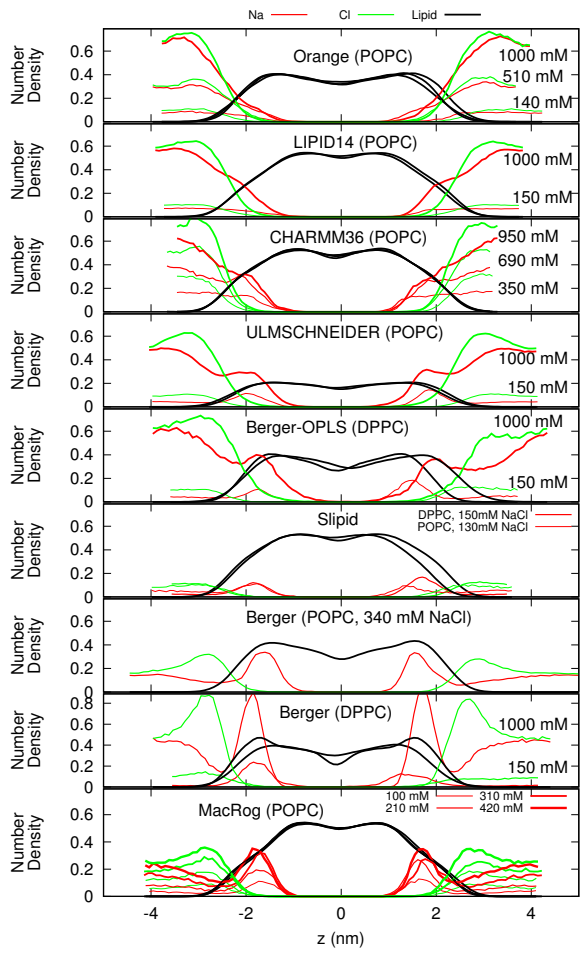

FIG. 5: Atom number density profiles along the membrane normal for lipids, Na^+, and Cl^- ions from simulations with different force fields and different NaCl concentrations. The force fields are ordered according to the order parameter changes reported Fig. 2, from the smallest (top panel) to the larges (bottom panel). The lipid densities are scaled by 100 (united atom) or 200 (all atom model) to improve readability. Figure discussed in https://github.com/NMRLipids/lipid_ionINTERACTION/issues/4.

analysis is required with current lipid models. Such analysis is performed in the next section.

C. Cation binding in different simulation models

The order parameter changes and density distributions in Figs. 2 and 5 with added NaCl show significantly different Na^+ binding affinities for different simulation models. The best agreement with experiments (i.e., lowest order parameter changes) is observed for the Orange, CHARMM36 and Lipid14 models (see Figs. 2). These also predict the lowest Na^+ densities in the proximity of the membrane (see Fig. 5). On the other hand, the choline order parameter changes with NaCl are clearly overestimated in all the other tested models (see Fig. 2) which also show stronger Na^+ binding affinity (see Fig. 5). Thus we conclude that the sodium binding affinity is overestimated in all the other models than Orange, CHARMM36 and Lipid14.

The order parameter changes with NaCl in the best three models are small (less than 0.02). Thus, with the achieved accuracy we cannot conclude which of these three models has the most realistic Na^+ binding affinity, especially with physiological NaCl concentrations ($\sim$ 150mM) which is relevant for most applications. The overestimated binding on the other models raise questions on the quality of the predictions from these models when NaCl is present. **4.It has been suggested that we should add references here. The problem is that there are a lot of them and it is difficult to choose which ones to pick. Any opinions?** Especially interactions between charged molecules and lipid bilayer might be significantly affected by the strong Na^+ binding which makes bilayer effectively positively charged.

As a function of $CaCl_2$ concentration, almost all the tested models overestimate the order parameter decrease, as seen in Fig. 2. The exception is the CHARMM36 with recent ion model by Yoo et al. [71]. According to the electrometer concept, the overestimated order parameter decrease indicates overestimated Ca^{2+} binding. This is the most likely scenario for the models where changes in both order parameters were overestimated, however, in the case of $CaCl_2$ we cannot exclude the explanation that the headgroup response is too sensitive for bound cations, see Supplementary Information. In CHARMM36 with ion model by Yoo et al. the order parameter decrease is overestimated for β but underestimated for α, in line with figure 3 where $\Delta S^{\beta}_{\mathrm{CH}}/\Delta S^{\alpha}_{\mathrm{CH}}$ ratio is larger in CHARMM36 than in experiments. Since we do not know if $\Delta S^{\beta}_{\mathrm{CH}}$ or $\Delta S^{\alpha}_{\mathrm{CH}}$ is more realistic in CHARMM36, we cannot conclude if Ca^{2+} binding is too strong or weak in this simulation. This could be resolved by comparing CHARMM36 model to the experimental data with known amount of bound charge (e.g. experiments with amphihilic cations [31, 46]), however, this is beyond the scope of the current work.

The ion density distributions with $CaCl_2$ in Fig. 6 show significant Ca^{2+} binding in all models, however, some difference occur between different models. The Berger model predicts deeper penetration depth (density maxima close to $\pm$1.8 nm) compared to other models (density maxima close to $\pm$2 nm). The latter value is probably more realistic since ^{1}H NMR and neutron scattering data indicates that Ca^{2+} interacts mainly with the choline group [3, 99–101]. In CHARMM36 model almost all Ca^{2+} ions present in simulation bind in bilayer indicating strongest binding affinity among the tested models. The difference is not as clear in Fig. 2 because α carbon order parameters are least sensitive to bound charge in CHARMM36 (Fig. 4).

Significant Ca^{2+} binding affinity to a phosphatidylcholine bilayer at mM concentrations is agreed in the literature [3, 4, 20, 30], however, several details are yet under discussion. Simulations suggest that Ca^{2+} bind to lipid carbonyl oxygens with coordination number of 4.2 [14], while interpretation of NMR and scattering experiments suggest that one Ca^{2+} interacts mainly with choline groups [99–101] of two phospholipid molecules [30]. Simulation model correctly reproducing the

TABLE I: List of simulations performed in this work. The ion concentrations are calculated as [ion]=($N_{ion}\times$[water])/N_w, where [water]=55.5M. These correspond the concentrations reported in the experiments by Akutsu et al. [20]. The lipid force fields are named as in our previous work [36].

Force field (lipid, ion)	lipid	[Ion] mM	[a]N_l	[b]N_w	[c]N_{Na}	[d]N_{Ca}	[e]N_{Cl}	[f]T (K)	[g]t_{sim}(ns)	[h]t_{anal} (ns)	Files
Berger-POPC-07[47]	POPC	0	128	7290	0	0	0	298	270	240	[48]
Berger-POPC-07[47], ffgmx[49]	POPC	340 (NaCl)	128	7202	44	0	44	298	110	50	[50]
Berger-POPC-07[47], ffgmx[49]	POPC	340 ($CaCl_2$)	128	7157	0	44	88	298	108	58	[51]
Berger-DPPC-97[52]	DPPC	0	72	2880	0	0	0	323	60	50	[53]
Berger-DPPC-97[52], ffgmx[49]	DPPC	150 (NaCl)	72	2880	8	0	8	323	120	60	[54]
Berger-DPPC-97[52], ffgmx[49]	DPPC	1000 (NaCl)	72	2778	51	0	51	323	120	60	[55]
BergerOPLS-DPPC-06[56]	DPPC	0	72	2880	0	0	0	323	120	60	[57]
BergerOPLS-DPPC-06[56], OPLS[58]	DPPC	150 (NaCl)	72	2880	8	0	8	323	120	60	[59]
BergerOPLS-DPPC-06[56], OPLS[58]	DPPC	1000 (NaCl)	72	2778	51	0	51	323	120	60	[60]
CHARMM36[61]	POPC	0	72	2242	0	0	0	303	30	20	[62]
CHARMM36[61], CHARMM36[63]	POPC	350 (NaCl)	72	2085	13	0	13	303	80	60	[64]
CHARMM36[61], CHARMM36[63]	POPC	690 (NaCl)	72	2085	26	0	26	303	73	60	[65]
CHARMM36[61], CHARMM36[63]	POPC	950 (NaCl)	72	2168	37	0	37	303	80	60	[66]
CHARMM36[61], CHARMM36	POPC	350 ($CaCl_2$)	128	6400	0	35	70	303	200	100	[67]
CHARMM36[61], CHARMM36	POPC	450 ($CaCl_2$)	200	9000	0	73	146	310	2000	100	[68]
CHARMM36[61], CHARMM36	POPC	670 ($CaCl_2$)	128	6400	0	67	134	303	200	120	[69]
CHARMM36[61], CHARMM36	POPC	1000 ($CaCl_2$)	128	6400	0	100	200	303	200	100	[70]
CHARMM36[61], Yoo[71]	DPPC	430 ($CaCl_2$)	128	7760	60	0	120	323	200	170	todo
CHARMM36[61], Yoo[71]	DPPC	886 ($CaCl_2$)	128	7520	120	0	240	323	200	170	todo
MacRog[72]	POPC	0	288	14400	0	0	0	310	90	40	[73]
MacRog[72], OPLS[58]	POPC	100 (NaCl)	288	14554	27	0	27	310	90	50	[74]
MacRog[72], OPLS[58]	POPC	210 (NaCl)	288	14500	54	0	54	310	90	50	[74]
MacRog[72], OPLS[58]	POPC	310 (NaCl)	288	14446	81	0	81	310	90	50	[74]
MacRog[72], OPLS[58]	POPC	420 (NaCl)	288	14392	108	0	108	310	90	50	[74]
Orange, OPLS[58]	POPC	0	72	2880	0	0	0	298	60	50	[75]
Orange, OPLS[58]	POPC	140 (NaCl)	72	2866	7	0	7	298	120	60	[76]
Orange, OPLS[58]	POPC	510 (NaCl)	72	2802	26	0	26	298	120	100	[77]
Orange, OPLS[58]	POPC	1000 (NaCl)	72	2780	50	0	50	298	120	80	[78]
Orange, OPLS	POPC	510 ($CaCl_2$)	72	2802	0	26	52	298	120	60	[79]
Slipid[80]	DPPC	0	128	3840	0	0	0	323	150	100	[81]
Slipid[80], AMBER[82, 83]	DPPC	150 (NaCl)	600	18000	49	0	49	323	100	40	-
Slipid[80], AMBER[82, 83]	DPPC	350 (NaCl)	3.JM, please fill these?	?	?	0	?	?	?	?	?
Slipid[80], AMBER[82, 83]	DPPC	700 (NaCl)	?	?	?	0	?	?	?	?	?
Slipid[80], AMBER[82, 83]	DPPC	1000 (NaCl)	?	?	?	0	?	?	?	?	?
Slipid[84]	POPC	0	128	5120	0	0	0	303	200	150	[85]
Slipid[84], AMBER[86]	POPC	130 (NaCl)	200	9000	21	0	21	310	105	100	[87]
Slipid[84], AMBER[58]	POPC	450 (CaCl)	200	9000	0	73	146	310	2000	100	[88]
Lipid14 [89], AMBER[58]	POPC	0	128	5120	0	0	0	298	205	200	[90]
Lipid14 [89], AMBER[58]	POPC	150 (NaCl)	128	5120	12	0	12	298	205	200	[91]
Lipid14 [89], AMBER[58]	POPC	1000 (NaCl)	128	5120	77	0	77	298	205	200	[92]
Lipid14 [89], AMBER[58]	POPC	350 ($CaCl_2$)	128	6400	0	35	70	298	200	100	[93]
Lipid14 [89], AMBER[58]	POPC	1000 ($CaCl_2$)	128	6400	0	100	200	298	200	100	[94]
Ulmschneiders [95], OPLS[58]	POPC	0	128	5120	0	0	0	298.15	205	200	[96]
Ulmschneiders [95], OPLS[58]	POPC	150 (NaCl)	128	5120	12	0	12	298.15	205	200	[97]
Ulmschneiders [95], OPLS[58]	POPC	1000 (NaCl)	128	5120	77	0	77	298.15	205	200	[98]

[a] The number of lipid molecules
[b] The number of water molecules
[c] The number of Na^+ molecules
[d] The number of Ca^{2+} molecules
[e] The number of Cl molecules
[f] Simulation temperature
[g] The total simulation time

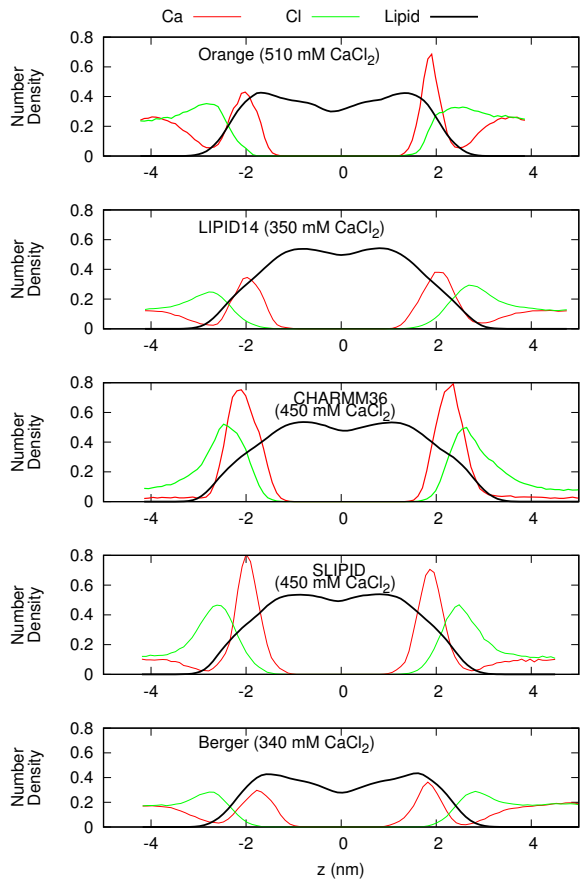

FIG. 6: Atom number density profiles along the membrane normal coordinate z for lipids, Ca^{2+} and Cl^- ions from simulations with different force fields. The profiles only with smallest available $CaCl_2$ concentration are shown for clarity. Figure including all the available concentrations is shown in the Supplementary Information. The lipid densities are scaled with 100 (united atom) or 200 (all atom model) to make them visible with the used y-axis scale. The Cl^- density is scaled with 2 to equalize charge density of ions. Figure discussed in https://github.com/NMRLipids/lipid_ionINTERACTION/issues/4.

order parameter changes would resolve the discussion by giving atomistic resolution interpretation for the experiments.

5.Stoichiometry discussion is updated.

The origin of inaccuracies in lipid-ion interactions and binding affinities in different models is far from clear. The potential candidates would be, for example, discrepancies in the ion models [102–104], incomplete treatment of electronic polarizability [105] or inaccuracies in lipid headgroup description [36]. Cordomi et al. [27] showed that Na^+ binding affinity decreases when ion radius increases in the model, however, also the models with largest radius show significant binding in DPPC bilayer simulated with OPLS-AA force field [106]. In our results the Slipid model gives essentially similar binding affinity with ion parameters from Refs. [86] and [82, 83]. Further, the compensation of missing electronic polarizability by scaling ion charge [105, 107] reduced Na^+ binding in Berger, BergerOPLS and Slipid models but not enough to be in agreement with experiments (see Supplementary Information). The charge scaled Ca^{2+} model [108] slightly reduced binding in CHARMM36 model but did not have significant influence on binding on Slipids model (see Supplementary Information). Significant reduction of Ca^{2+} binding was observed with ion model by Yoo et al [71], however, the CHARMM36 lipid model must be further analyzed to fully interpret the results.

On the other hand, also the lipid models may have significant influence on ion binding behaviour. For example, the same ion model and non–bonded parameters are used in the Orange and BergerOPLS [56] simulations, but while Na^+ ion binding affinity is realistic in the Orange model, it is seriously overestimated in the BergerOPLS (Fig. 5). However, the realistic Na^+ binding do not directly relate to realistic Ca^{2+} binding (see Orange, Lipid14 and CHARMM36 in Fig. 2) or realistic choline order parameter response in bound charge (see Orange and CHARMM36 in Fig. 3). It should be also noted that the low binding affinity of Na^+ in CHARMM36 model is due to the additional repulsion added between sodium ions and lipid oxygens (NBFIX) [63] (see supplementary information). Altogether, our results indicate that probably both, lipid and ion force field parameters, need improvement to correctly predict the cation binding affinity.

III. CONCLUSIONS

As suggested by the molecular electrometer concept [1, 20, 30, 31], the decrease in order parameters of α and β carbons in the PC head group of lipids bilayers is related to cation binding in all tested simulation models, despite of inaccuracies in actual atomistic resolution structures [36]. The concept allows direct comparison of Na^+ binding affinity between simulations and NMR experiments by using changes in the head group order parameter. The comparison reveals that most models overestimate the Na^+ binding; only Orange, Lipid14, and CHARMM36 predict realistic binding affinity. None of the tested models has the required accuracy to interpret the Ca^{2+}/lipid stoichiometry or induced structural changes with atomistic resolution.

In general, our results support the traditional (pre-2000) view that Na^+ and other monovalent ions (bar Li^+) do not specifically bind to the phospholipid bilayer at mM concentrations, in contrast to Ca^{2+} and other multivalent ions [2, 5, 11, 12, 20–22, 30]. The contradicting results from previous molecular dynamics simulations [13, 14], fluorescent probe dynamics [8, 10, 13], calorimetry [9, 13] and AFM [15–19], suggesting stronger Na^+ binding, can be explained by simulation artefacts, direct interactions between Na^+ and fluorescent probes [12], alternative interpretations of the significance of small phase transition temperature shifts [3], and insufficient resolution of AFM.

The artificial specific Na^+ binding in simulations may lead to doubtful results, since it effectively leads to positively charged phoshatidylcholine (PC) lipid bilayers even at physiological NaCl concentration. Such PC bilayer has distinctly

different interactions with charged objects compared to the more realistic model without specific Na^+ binding. Furthermore, the overestimation of Na^+ binding affinity may extend also to other positively charged objects, e.g. membrane protein segments. This would affect lipid protein interactions and could explain contradicting results on electrostatic interactions between charged protein segments and lipid bilayer [109, 110]. In conclusion, more careful studies and model development on lipid bilayer–charged object interactions are needed to make molecular dynamics simulations directly usable in physiologically relevant electrostatic environment.

This work has been, and will be, progressed and discussed through the blog `nmrlipids.blogspot.fi`, through which everyone is invited to join the discussion and make contributions. The manuscript will be eventually submitted to an appropriate scientific journal. Everyone who has contributed to the work through the blog will be offered coauthorship. For more details see `nmrlipids.blogspot.fi`.

Acknowledgements: OHSO acknowledges Tiago Ferreira for very useful discussions, the Emil Aaltonen foundation for financial support, Aalto Science-IT project and CSC-IT Center for Science for computational resources. MSM acknowledges financial support from the Volkswagen Foundation (86110). M.G. acknowledges financial support from Finnish Center of International Mobility (Fellowship TM-9363). J. M. acknowledges computational resources provided by the CESNET LM2015042 and the CERIT Scientific Cloud LM2015085 projects under the program "Projects of Large Research, Development, and Innovations Infrastructure"

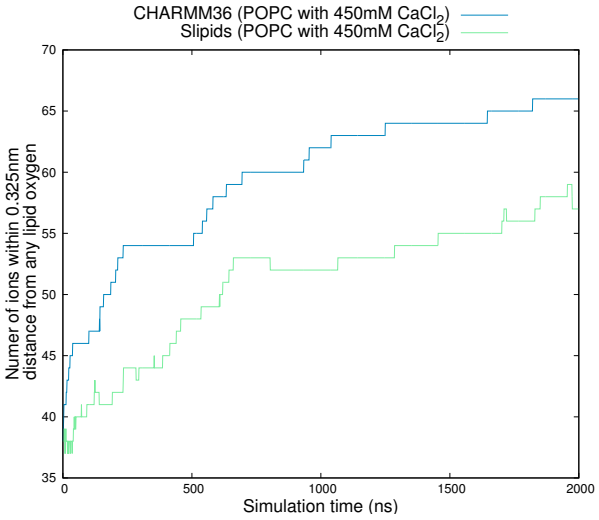

FIG. 7: Number of bound Ca^{2+} as a function of time from 2 μ long simulations with CHARMM36 and Slipids.

SUPPLEMENTARY INFORMATION

Appendix A: Ion binding equilibration times

Simulations containg 450 mM $CaCl_2$ with CHARMM36 and Slipids were ran 2 μs to estimate the times required to equilibrate amount of bound Ca^{2+} in lipid bilayer. The amount of the bound Calcium as a function of simulation time from these simulations are shown in Fig. 7. The results show clear increase in binding affinity up to 1000 ns and 700 ns in CHARMM36 and Slipids, respectively, and moderate increase even after this. This is also reflected to the CHARMM36 results in Fig. 2, where long CHARMM36 simulation with 450 mM $CaCl_2$ show relatively lower order parameters than shorter simulations. This can be rationalized with higher and more equilibrated binding affinity in long simulations. The results suggest that in other simulations the binding affinity is underestimated due to the insufficient equilibration times. This should be taken into account in more careful studies, but do not interfere the conclusion in this work that Ca^{2+} binding is most likely overestimated in all the other models than in possibly in CHARMM36 with ion model by Yoo et al. [71].

Appendix B: Headgroup response on charged amphiphiles

The order parameter changes as a function of bound charge cannot be straightforwardly compared between simulations and experiments from systems with ions because the results depend on the definition of bound ions in simulatios. In systems with charged amphihiles the situation is more straightforward since all the charges can be assumed to locate in bilayer in both, simulations and experiments. The order parameter changes as a function of charged amphiphiles, calculated

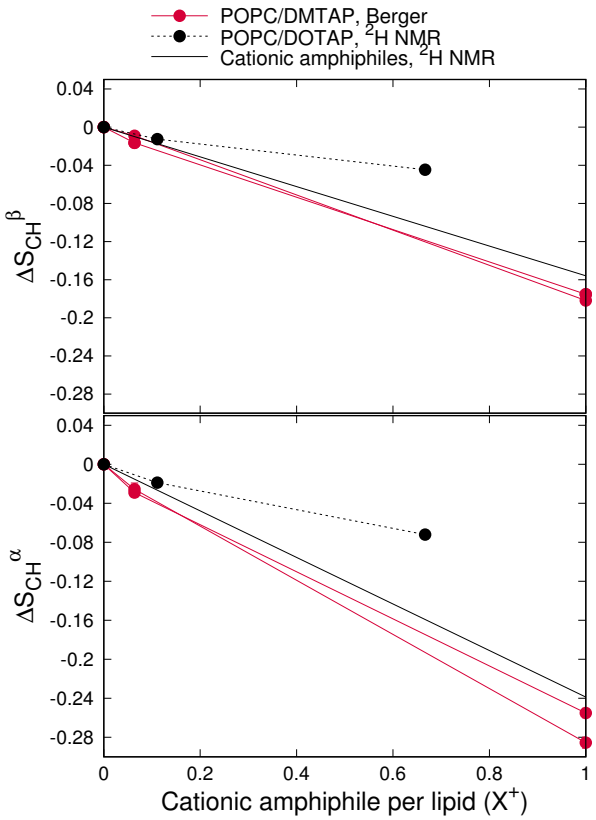

FIG. 8: Order parameter changes as a function of cationic amphihiles from simulations [45, 111–113] and experiments [31, 46]. Experimental points for binary mixtures of POPC and 1,2-dioleoyloxy-3-(trimethylammonio)propane (DOTAP) are from [46]. Experimental lines are from $\Delta S^i_{\mathrm{CH}} = \frac{4}{3}\chi^{-1} m_i X^{\pm}$, where m_i are taken as average for different amphiphiles measured in [31].

from previously published simulation data [45, 111–113] and experiments [31, 46], is shown in Fig 8.

The simulation data is from previously published binary mixture of cationic dimyristoyltrimethylammoniumpropane (DMTAP) and zwitterionic (neutral) dimyristoylphosphatidylcholine (DMPC) [45, 111–113], simulated with Berger based model. This is compared to experimental data from binary mixtures of POPC and various cationic amphiphiles [31, 46].

The order parameter changes from simulations are in good agreement with experimental line from various amphiphiles measured by Scherer et al. [31] but overestimate the changes measured from DMPC/DOTAP mixtures [46], especially with larger amphiphile concentrations. It is not clear if the overestimation comes from too sensitive headgroup, differences in the location of charge in bilayer or difference between DMTAP and DOTAP (DOTAP has two double bonds in acyl chains while DMTAP has two saturated chains). Assuming area per lipid 0.68 nm^2 and estimating the maximum amount of bound charge per lipid in simulations from Fig. 4 ($X^+_{\mathrm{max}} = 0.5\frac{\mathrm{q}}{\mathrm{nm}^2} \cdot 0.68\mathrm{nm}^2 = 0.34\frac{\mathrm{q}}{\mathrm{lipid}}$) gives maximum overestimations of ≈0.04 and ≈0.06 for β and α order parameter changes, respectively, with largest amount of bound cations in simulations. The numbers are smaller with less amount of bound cations. In principle, these value could explain the overestimated order parameter change due to the presence of $CaCl_2$ in Berger model but not in the presense of NaCl (see Fig. 2).

In conclusion, with the current data we cannot fully exclude the possibility that the overestimated order parameter response to the $CaCl_2$ with Berger model arises from oversensitive headgroup response to bound cations. However, in the presense of NaCl the differences between responses in simulations and experiments in Fig. 2 are larger than the maximum estimated influence from oversensitivity of headgroup.

Appendix C: Density distributions with different $CaCl_2$ concentrations

The density distributions with all simulated $CaCl_2$ concentrations are shown in Fig. 9.

Appendix D: Effect of ion model and polarization

It has been suggested that the missing electronic polarizability can be compensated by scaling the ion charge in simulations [105]. To test if this would improve the Na^+ ion binding behaviour, we ran simulations with Berger-DPPC-97, BergerOPLS-DPPC-06 and Slipids with scaled Na^+ and Cl^- ions. For Berger-DPPC-97 and BergerOPLS-DPPC-06 models the ion charge in systems listed in Table I was simply scaled with 0.7 and the related files are available at [114–117]). For simulations with Slipids the ion model by Kohagen et al. was used [107] and the related files are available at [118]. The simulation parameters were identical to those employed in the simulation of POPC with 130 mM NaCl (see Methods). The order parameter changes and Na^+-binding affinity are decreased by the charge scaling but yet overestimated with respect to the experiments as seen from Figs. 10 and 11. Thus the overestimated binding affinity cannot be fixed by only scaling charges.

The ion model for $CaCl_2$ with scaled charges [108] was tested with CHARMM36 and Slipid models. The related files are available at [119] and [120], respectively, and the results are shown in Figs. 10 and 9. The results with scaled charges are slightly improved but yet far from experiments.

Figure 10 also compares CHARMM36 simulation with and without NBFIX [63] for NaCl. As expected, without NBFIX the order parameter decrease is more significant. **6.Discussion will be finished as soon as we have the density profiles. Citations to Zenodo repositories will be added, if available.**

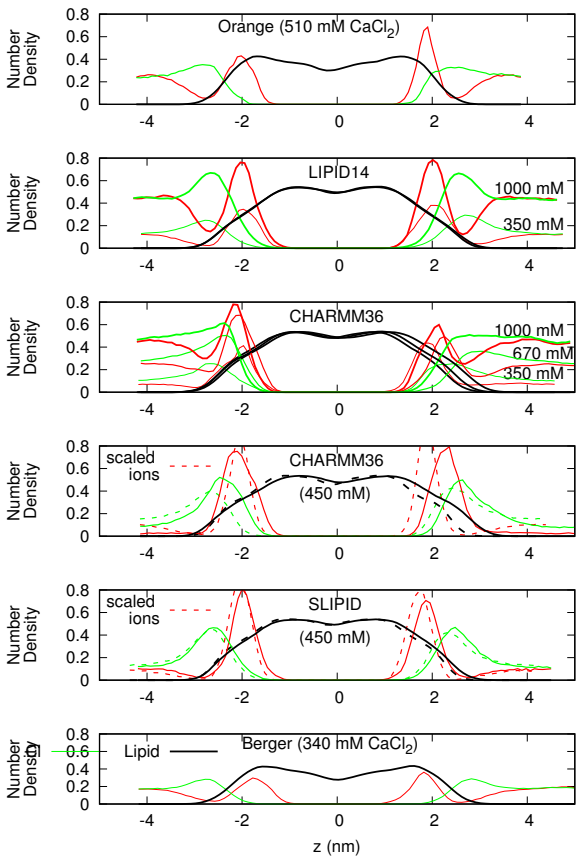

FIG. 9: Number density profiles for lipids, Ca^{2+} and Cl^- ions from simulations with different force fields and different $CaCl_2$ concentrations. The lipid densities are scaled with 100 (united atom) or 200 (all atom model) to make them visible with the used y-axis scale. The Cl^- density is scaled with 2 to equalize charge density of ions. Figure discussed in https://github.com/NMRLipids/lipid_ionINTERACTION/issues/4.

Appendix E: methods

1. Simulated systems

All simulations are ran with a standard setup for planar lipid bilayer in zero tension with periodic boundary conditions with Gromacs software package (version numbers 4.5-X-5.0.X).

2. Analysis

The order parameters were calculated from simulation trajectories directly applying the equation $S_{\mathrm{CH}} = \langle \frac{3}{2}\cos^2\theta - \frac{1}{2} \rangle$, where θ is the angle between a given C–H bond and the bilayer normal and average is taken over all lipids and time frames. For united atom models, the positions of hydrogen atoms were calculated for each molecule in each frame *a posteriori* by using the *protonate* tool in Gromacs 4.0.2 [121]. The statistical error in the order parameter was estimated by calculating the average value separately for each lipid molecule, and then the average and standard error of the mean over the ensemble of lipids (as done also in previous work [36]). All the scripts used in analysis and the resulting data are available in the GitHub repository [122]

3. Simulation details

a. *Berger*

POPC The simulation without ions is the same as in [123] and the files are available at [48]. The starting structures for simulations with ions is made by replacing water molecules with appropriate amount of ions (see Table I). The Berger force field was used for the POPC [124], with the dihedral potential next to the double bond taken from [125]. The ion parameters from ffmgx [49] were used. Timestep of 2 fs was used with leap-frog integrator. Covalent bond lengths were constrained with LINCS algorithm [126, 127]. Coordinates were written every 10 ps. PME [128, 129] with real space cut-off 1.0 nm was used for electrostatics. Plain cut-off was used for the Lennard-Jones interactions with a 1.0 nm cut-off. The neighbour list was updated every 5th step with cut-off 1.0 nm. Temperature was coupled separately for lipids, water and ions to 298 K with the velocity-rescale method [130] with coupling constant 0.1 ps^{-1}. Pressure was semi-isotropically coupled to the athmospheric pressure with the Parrinello-Rahman barostat [131].

DPPC The simulation without ions is the same as in [36] and the files are available at [53]. The initial configuration contained 72 DPPC lipids and 2880 SPC water molecules. The standard Berger DPPC force field was used [124] (simulations indicated as Berger-DPPC-97 in Table I). The electrostatics were handled with PME [128, 129], with real-space Coulomb cut-off set at 1.0 nm. Lennard-Jones potentials were cut off 1.0 nm. The neighborlist for all non-bonded interactions was updated every 10 steps. Temperature was set to 323K with the velocity-rescale method [130] using a coupling constant of 0.1 ps^{-1}. Semi-isotropic pressure coupling at 1 ATM was handled with the Parrinello-Rahman barostat [131] with 1 ps coupling constant. The time step was 4 fs, and coordinates were written every 10 ps. The total simulation time was 120 ns (without pre-equilibration) and last 60 ns was used in the order parameter analysis.

For simulations with added salt, the appropriate number of SPC water molecules were randomly replaced with ions. Ions were described by the ffgmx parameters [49]. In simulations with scaled charges, charge-scaling was applied by scaling the ion charges by a factor 0.7. Conditions in the ion simulations were as with the pure DPPC described above. The duration of the simulations was 120 ns (without pre-equilibration) and last 60 ns was used in the order parameter analysis.

All the simulation files for pure DPPC simulations can be found at [53] and for the simulations with ions at [54, 55] and with scaled ions at [114, 115].

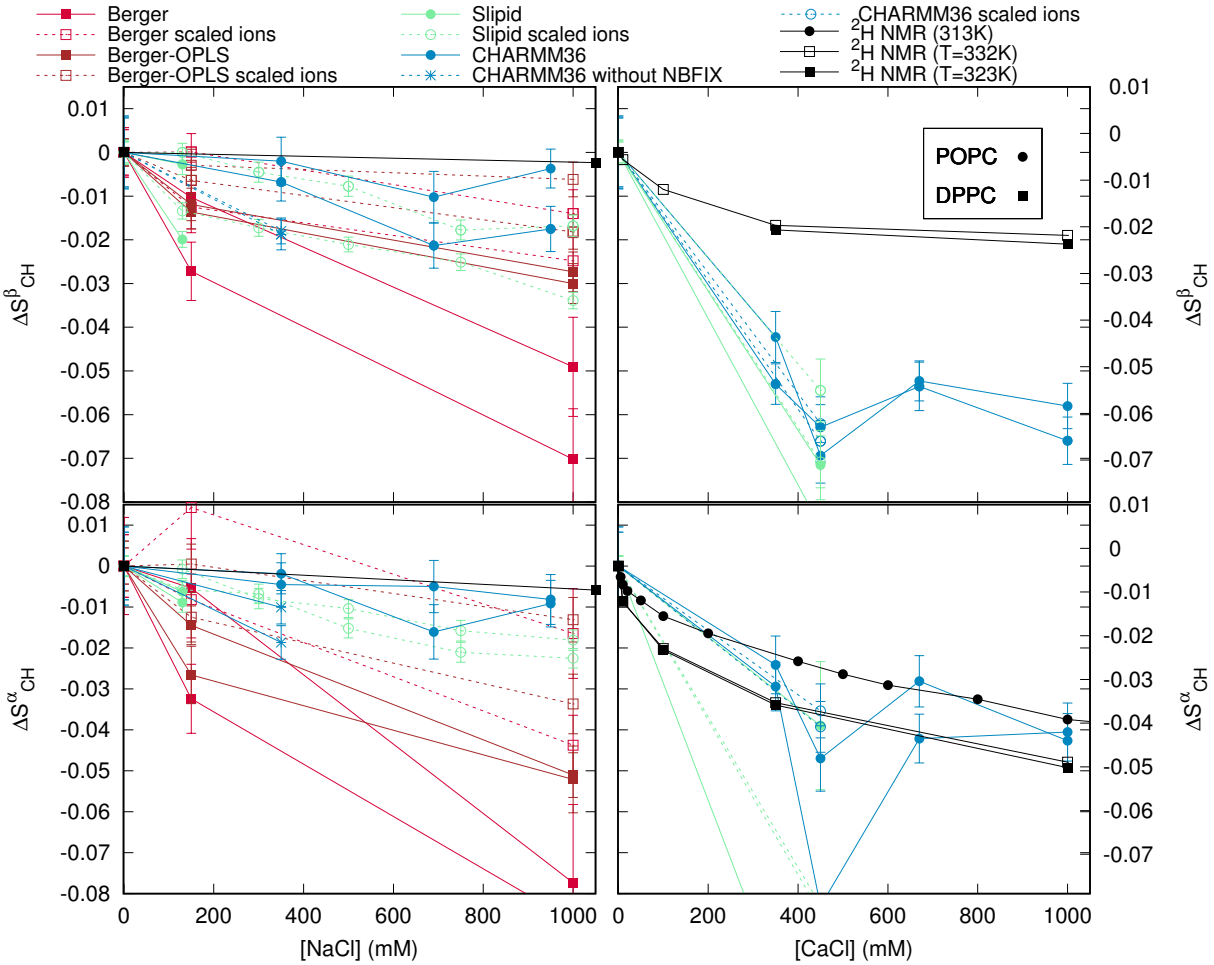

FIG. 10: The effect of charge scaling [105, 108] and NBFIX [63] on order parameter changes in simulations.

b. BergerOPLS

c. CHARMM36

For simulations without ions, the initial configuration contains 72 DPPC lipids and 2880 SPC water molecules. For simulations with added salt, the appropriate amount of SPC water molecules were randomly replaced with ions. The number of ions is reported in Table I. For the lipids, we used the same version of Berger force field as in previous simulations, described in [124]; for the ions, we used the qvist parameters [58] (commonly used within the OPLS-AA force field). Issues related to the compatibility between Berger and OPLS-AA force fields are described in ref. [56]. A set of simulations was carried out using reduced electrostatic charges on the ions; in this case, a charge of 0.7 e was used on the ions, as described in refs. [105, 107]. Except for the ion force field, all simulation parameters (for non-bonded interactions, integration time step, thermostat, etc.) were identical to the parameters used in the Berger DPPC simulations described above.

All simulation files can be found at [57] for pure DPPC simulations, at [59, 60] for simulations with ions, and at [116, 117] for simulations with ions with scaled charges.

POPC with NaCl The simulation without ions is taken directly from [36, 62]. The starting structures for simulations with NaCl were made by replacing randomly located water molecules of the structure of pure POPC simulation with appropriate amount of ions. The force field for lipid were the same as in [36, 62]. The ion parameters with NBFIX by Venable et al. [63] were used. Simulations were ran with Gromacs 4.5.5 software [132]. Timestep of 2 fs was used with leap-frog integrator. Covalent bonds with hydrogens were constrained with LINCS algorithm [126, 127]. Coordinates were written every 5 ps. PME with real space cut-off 1.4 nm was used for electrostatics. Lennard-Jones interactions were switched to zero between 0.8 nm and 1.2 nm. The neighbour list was updated every 5th step with cut-off 1.4 nm. Temperature was coupled separately for lipids and solution to 303 K with the velocity-rescale method [130] with coupling constant 0.2 ps. Pressure was semi-isotropically coupled to the athmospheric pressure with the Berendsen method [133].

Also simulation without NBFIX [63] was run to check its effect on Na^+ binding. **7.JM, please add the details here**

POPC with $CaCl_2$ The starting structures with vary-

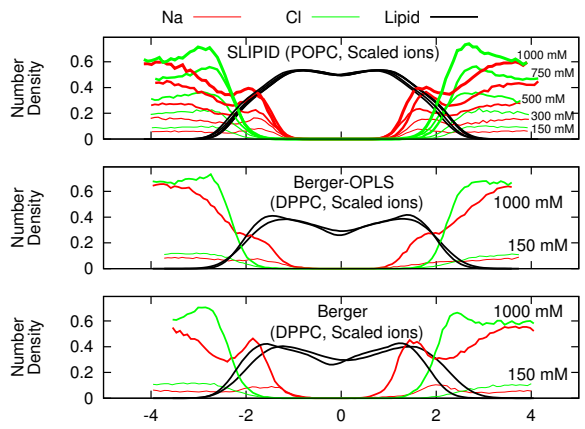

FIG. 11: Atom number density profiles along membrane normal coordinate z for lipids, Na^+ and Cl^- ions from simulations using ion models with scaled charges. The lipid densities are scaled with 100 (united atom) or 200 (all atom model) to make them visible with the used y-axis scale.

ing amounts of $CaCl_2$ ions were constructed using the CHARMM-GUI Membrane Builder (http://www.charmm-gui.org/) online tool [134]. All runs were performed with Gromacs 5.0.3 software package [135] and CHARMM36 additive force field parameters for lipids [61] and ions were obtained from CHARMM-GUI input files. Standard CHARMM-GUI mdp options were used. Particularly, h-bond lengths were constrained with LINCS [126, 127]. The temperatures of the lipids and the solvent were separately coupled to the Nose-Hoover [136, 137] thermostat with a target temperature of 303 K and a relaxation time constant of 1.0 ps. Semi-isotropical pressure coupling to 1 bar was obtained with the Parrinello-Rahman barostat [131] with a time constant of 5 ps. Equations of motion were integrated with the Verlet algorithm [138] using a timestep of 2 fs. Long-range electrostatic interactions were calculated using the PME [128, 129] method with a fourth order smoothing spline. A real space cut-off of 1.2 nm was employed with grid spacing of 0.12 nm in the reciprocal space. Lennard-Jones interactions were smoothly switched to zero between 1.0 nm and 1.2 nm. Verlet cutoff-scheme [138] were used with the long-range neighbor list updated every 20 steps. Coordinates were written every 10 ps. After energy minimization and an equilibration run of 0.5 ns, 200ns simulations were ran and the last 100ns of each simulation was employed for the analysis.

DPPC with $CaCl_2$ (Yoo model) The systems contained 128 DPPC lipids and about 7600 TIP3P water molecules, and an appropriate amount of ions as indicated in Table I. We have used CHARMM36 additive force field parameters for lipids [61]. In the calcium model developed recently by Yoo et al. in [71], each cation is decorated by seven hydrating water molecules (with different charges from the usual TIP3P), which are constrainted to remain in its vincinity. The associated parameter files was available on http://bionano.physics.illinois.edu/CUFIX. The constraint on the Calcium-Oxygen distances was imposed by adding extra-bonds through a harmonic potential $V(r) = k * (r - r_0)^2$, with $r_0 = 2.25$ Åand $k = 10$ kcal·mol^{-1}·Å^{-2}.

The starting configuration of hydrated lipidic bilayers were constructed using packmol package [139] with a large area par lipid (74 Å^2). After a first energy minimization (5000 steps), varying amounts of $CaCl_2$ ions were added by replacing water molecules, using the autoionize plugin of vmd package [140], mentionning explicitely the number of ions required. Ion placement is random, with the constraint of minimum 5 Åbetween ions and lipids, as well as between any two ions. A second energy minimization was performed after inserting the ions.

All the minimizations and dynamics were conducted using the NAMD package developed by the Theoretical and Computational Biophysics Group at the University of Illinois at Urbana-Champaign [141]. The temperature of the whole system was controled thanks to a Langevin thermostat with a target temperature of 323 K and a relaxation time constant of 1 ps. The modified NAMD version of the NoseHoover barostat with Langevin dynamics (piston period of 0.1 ps and piston decay time of 0.05 ps) was used semi-isotropically to reach the averaged target pressure of 1 bar and an averaged zero surface tension. The ratio of the box length in $x-$ and $y-$ directions was kept fixed to avoid spurious box anisotropy. The equations of motion were integrated using the multiple time step Verlet r-RESPA algorithm [138] with a time step of 2 fs, and electrostatic forces calculated only every two timesteps. Covalent bonds between heavy and hydrogen atoms were constrained using SHAKE/RATTLE algorithm. Long-range electrostatic interactions were calculated using the PME [128, 129] method with a 4-th order smoothing spline and a grid spacing of about 0.1 nm. A cut-off of 1.2 nm was employed for the Lennard-Jones interactions, with a force-based switching function for distances beyond 1 nm. Neighbor lists with a radius of 1.4 nm were updated every 10 timesteps. The temperature was kept at 323 K with a Langevin thermostat with a damping coefficient of 5 ps. Coordinates were written every 20 ps. After energy minimization, a run of 200 ns simulations was performed. About 30 ns of trajectory was eliminated, and the last $\sim$ 170 ns of trajectory was employed for the analysis. Error bars are defined by +/- the standard error of the mean, taking into account the correlation time of the average order parameters (200 ps for 430 mM and 400 ps for 890 mM).

d. MacRog

The simulation parameters are identical to those employed in our earlier study [36] for the full hydration and dehydration simulations. The initial structures with varying amounts of NaCl were constructed from an extensively hydrated bilayer by replacing water molecules with ions using the Gromacs tool genion [142]. Even at the highest considered salt concentration, the amount of water molecules per lipid after this replacement process was still greater than 50.

e. Orange

The systems contained 72 POPC lipids and 2880 SPC water molecules, and an appropriate amount of ions as indicated in Table I.

For the lipids, we used an unpublished force field coined Orange force field. Briefly, this includes most bonded interactions from Berger lipids [124], except for dihedrals which were derived via *ab initio* calculations on small model compounds. As in Berger lipids, Lennard-Jones parameters are from OPLS [143–147]. Partial charges were derived on the basis of *ab initio* calculations. In simulations with ions, the qvist parameters were used [58]. The electrostatics were handled with PME [128, 129], with real-space Coulomb cut-off set at 1.8 nm. Lennard-Jones potentials were cut off at 1.8 nm. The neighborlists for the calculation of non-bonded forces were updated every 5 steps.

Temperature was set to 298K with the velocity-rescale thermostat [130] using a coupling constant of 0.1 ps^{-1}, and the pressure was set to 1 bar using the Berendsen weak coupling algorithm [133] (compressibility of 4.5*10$^-$5 bar$^-$1, time constant of 1 ps), coupling separately the x-y dimension and the z dimension to obtain a tensionless system. A time step of 2 fs was used for the integration (with the leap-frog algorithm), coordinates were written every 100 ps, and the total simulation time was 60 ns.

Simulation files for pure lipid simulations are found at [75] and for the simulations with ions at [76–79].

f. Slipids

DPPC The simulation without ions from [36], available at [81] was used. For the simulations with ions, the starting DPPC lipid bilayer, which was built with the online CHARMM-GUI [134] (http://www.charmm-gui.org/), contained 600 lipids, 30 water molecules/lipid, Na^+ and Cl^- ions (150 mM NaCl). The TIP3P water model was used to solvate the system and ion parameters by Roux [82, 83] were used. the GROMACS software package version 4.5.5 [132] and the Stockholm lipids (Slipids) force field parameters for phospholipids were used. After energy minimization and a short equilibration run of 50 ps (time step 1 fs), 100 ns production runs were performed using a time step of 2 fs with leap-frog integrator. All covalent bonds were constrained with the LINCS [126, 127] algorithm. Coordinates were written every 100 ps. PME [128, 129] with real space cut-off at 1.0 nm was used for Coulomb interactions. Lennard-Jones interactions were switched to zero between 1.0 nm and 1.4 nm. The neighbour lists were updated every 10^{th} step with a cut-off of 1.6 nm. Temperature was coupled separately for upper and bottom leaflets of the lipid bilayer, and for water to one of the temperatures reported above with the Nosé-Hoover thermostat [136, 137] using a time constant of 0.5 ps. Pressure was semi-isotropically coupled to the atmospheric pressure with the Parrinello-Rahman [131] barostat using a time constant of 10 ps. **8.JM, please add description of the new data**

POPC The simulation without ions from [36], available at [85] was used. Additionally, a POPC bilayer consisting of 200 lipids, hydrated with 45 water molecules per lipid, was simulated in the presence of 130 mM NaCl. **9.Details from the simulation with CaCl** The Slipids model [80, 84] was employed for lipids, the tip3p model [148] for water, and the ion parameters by Smith and Dang [86] for NaCl. The system was first equilibrated for 5 ns with a time step of 1 fs after which a 100 ns production run was performed using a time step of 2 fs. Trajectories were written every 100 ps. The system was kept in a tensionless state at 1 bar using a semi-isotropical Parrinello–Rahman barostat [131] with a time constant of 1 ps. The temperature was maintained at 310 K with the velocity rescaling thermostat [130]. The time constant was set to 0.5 ps for both lipids and solvent (water and ions) which were coupled separately. Non-bonded interactions were calculated within a neighbor list with a radius of 1 nm and an update interval of 10 steps. The Lennard-Jones interactions were cut-off at 1 nm, whereas PME [128, 129] was employed for long-range electrostatics. Dispersion correction was applied to both energy and pressure. All bonds were constrained with the LINCS [126, 127]. algorithm.

g. Lipid14

The starting structures with varying amounts of ions were constructed using the CHARMM-GUI Membrane Builder (http://www.charmm-gui.org/) online tool [134]. The GROMACS compatible force field parameters generated in [36] and available at [149] were used. The TIP3P water model [148] was used to solvate the system and Åqvist [58] parameters were used for ions. All runs were performed with Gromacs 5.0.3 software package [135] and LIPID14 force field parameters for POPC [89].

H-bond lengths were constrained with LINCS [126, 127]. The temperatures of the lipids and the solvent were separately coupled to the Nose-Hoover [136, 137] thermostat with a target temperature of 298.15 K and a relaxation time constant of 0.1 ps. Semi-isotropical pressure coupling to 1 bar was obtained with the Parrinello-Rahman barostat [131] with a time constant of 2 ps. Equations of motion were integrated with the Verlet algorithm [138] using a timestep of 2 fs. Long-range electrostatic interactions were calculated using the PME [128, 129] method with a fourth order smoothing spline. A real space cut-off of 1.0 nm was employed with grid spacing of 0.12 nm in the reciprocal space. Lennard-Jones potentials were cut-off at 1 nm, with a dispersion correction applied to both energy and pressure. Verlet cutoff-scheme [138] were used with the long-range neighbor list updated every 20 steps. Coordinates were written every 10 ps.

After energy minimization and an equilibration run of 5 ns, 200ns production runs were performed and analysed. In case of the CaCl2 systems only the last 100ns of each simulation was employed for the analysis.

h. Ulmschneiders

The starting structures with varying amounts of ions were constructed using the CHARMM-GUI Membrane Builder (`http://www.charmm-gui.org`) online tool [134]. The force field parameters were obtained from Lipidbook [150]. The TIP3P water model [148] was used to solvate the system. Additionally, the simulations of ion-free bilayer were repeated with both Verlet and Group cutoff-schemes [96]. There was no significant difference in headgroup or glycerol backbone order parameters between these cutoff-schemes. All runs were performed with Gromacs 5.0.3 software package [135]. The glycerol backbone order parameters without iones were not the same as reported in the previous study [36]. The origin of discrepancy was located to the different initial structures which was taken from CHARMM-GUI in this work and from Lipidbook in the previous work. Since the order parameters with the initial structure from CHARMM-GUI are closer to the experimental values, the results indicate that the structure available from Lipidbook is stuck to a state with incorrect glycerol backbone structure, for more discussion see `https://github.com/NMRLipids/lipid_ionINTERACTION/issues/8`.

All-bond lengths were constrained with LINCS [126, 127]. The temperatures of the lipids and the solvent were separately coupled to the Nose-Hoover [136, 137] thermostat with a target temperature of 298.15 K and a relaxation time constant of 0.1 ps. Semi-isotropical pressure coupling to 1 bar was obtained with the Parrinello-Rahman barostat [131] with a time constant of 2 ps. Equations of motion were integrated with the Verlet algorithm [138] using a timestep of 2 fs. Long-range electrostatic interactions were calculated using the PME [128, 129] method with a fourth order smoothing spline. A real space cut-off of 1.0 nm was employed with grid spacing of 0.12 nm in the reciprocal space. Lennard-Jones potentials were cut-off at 1 nm, with a dispersion correction applied to both energy and pressure. Verlet cutoff-scheme [138] were used with the long-range neighbor list updated every 20 steps. Coordinates were written every 10 ps. After energy minimization and an equilibration run of 5 ns, 200ns simulations were ran and the last 100ns of each simulation was employed for the analysis.

Appendix F: Author Contributions

Andrea Catte
Mykhailo Girych ran and analyzed several simulations. Discussed the project actively with OHSO.
Matti Javanainen provided data with several lipid and ion models. Discussed the project actively with OHSO. Supervised the work of JT.
Claire Loison
Josef Melcr
Markus S. Miettinen
Luca Monticelli
Jukka Määttä
Vasily S. Oganesyan
O. H. Samuli Ollila co-designed the project with MSM and managed the work. Ran and analyzed several simulations. Wrote the manuscript.
Joona Tynkkynen
Sergey Vilov

TODO

P.

[1] J. Seelig, P. M. MacDonald, and P. G. Scherer, Biochemistry **26**, 7535 (1987).
[2] M. Eisenberg, T. Gresalfi, T. Riccio, and S. McLaughlin, Biochemistry **18**, 5213 (1979).
[3] G. Cevc, Biochim. Biophys. Acta - Rev. Biomemb. **1031**, 311 (1990).
[4] J.-F. Tocanne and J. Teissi, Biochimica et Biophysica Acta (BBA) - Reviews on Biomembranes **1031**, 111 (1990).
[5] H. Binder and O. Zschörnig, Chem. Phys. Lipids **115**, 39 (2002).
[6] J. J. Garcia-Celma, L. Hatahet, W. Kunz, and K. Fendler, Langmuir **23**, 10074 (2007).
[7] E. Leontidis and A. Aroti, The Journal of Physical Chemistry B **113**, 1460 (2009).
[8] R. Vacha, S. W. I. Siu, M. Petrov, R. A. Böckmann, J. Barucha-Kraszewska, P. Jurkiewicz, M. Hof, M. L. Berkowitz, and P. Jungwirth, J. Phys. Chem. A **113**, 7235 (2009).
[9] B. Klasczyk, V. Knecht, R. Lipowsky, and R. Dimova, Langmuir **26**, 18951 (2010).
[10] F. F. Harb and B. Tinland, Langmuir **29**, 5540 (2013).

[11] G. Pabst, A. Hodzic, J. Strancar, S. Danner, M. Rappolt, and P. Laggner, Biophys. J. **93**, 2688 (2007).

[12] A. Filippov, G. Ordd, and G. Lindblom, Chemistry and Physics of Lipids **159**, 81 (2009).

[13] R. A. Böckmann, A. Hac, T. Heimburg, and H. Grubmüller, Biophys. J. **85**, 1647 (2003).

[14] R. A. Böckmann and H. Grubmüller, Ang. Chem. Int. Ed. **43**, 1021 (2004).

[15] S. Garcia-Manyes, G. Oncins, and F. Sanz, Biophys. J. **89**, 1812 (2005).

[16] S. Garcia-Manyes, G. Oncins, and F. Sanz, Electrochimica Acta **51**, 5029 (2006), ISSN 0013-4686, bioelectrochemistry 2005 Bioelectrochemistry 2005, URL http://www.sciencedirect.com/science/article/pii/S0013468606002775.

[17] T. Fukuma, M. J. Higgins, and S. P. Jarvis, Phys. Rev. Lett. **98**, 106101 (2007).

[18] U. Ferber, G. Kaggwa, and S. Jarvis, European Biophysics Journal **40**, 329 (2011), ISSN 0175-7571, URL http://dx.doi.org/10.1007/s00249-010-0650-7.

[19] L. Redondo-Morata, G. Oncins, and F. Sanz, Biophysical Journal **102**, 66 (2012).

[20] H. Akutsu and J. Seelig, Biochemistry **20**, 7366 (1981).

[21] R. J. Clarke and C. Lpfert, Biophysical Journal **76**, 2614 (1999).

[22] S. A. TATULIAN, European Journal of Biochemistry **170**, 413 (1987), ISSN 1432-1033, URL http://dx.doi.org/10.1111/j.1432-1033.1987.tb13715.x.

[23] M. L. Berkowitz, D. L. Bostick, and S. Pandit, Chem. Rev. **106**, 1527 (2006).

[24] V. Knecht and B. Klasczyk, Biophys. J. **104**, 818 (2013).

[25] J. N. Sachs, H. Nanda, H. I. Petrache, and T. B. Woolf, Biophys. J. **86**, 3772 (2004).

[26] A. Cordom, O. Edholm, and J. J. Perez, The Journal of Physical Chemistry B **112**, 1397 (2008).

[27] A. Cordomi, O. Edholm, and J. J. Perez, J. Chem. Theo. Comput. **5**, 2125 (2009).

[28] C. Valley, J. Perlmutter, A. Braun, and J. Sachs, J. Membr. Biol. **244**, 35 (2011).

[29] M. L. Berkowitz and R. Vacha, Acc. Chem. Res. **45**, 74 (2012).

[30] C. Altenbach and J. Seelig, Biochemistry **23**, 3913 (1984).

[31] P. G. Scherer and J. Seelig, Biochemistry **28**, 7720 (1989).

[32] O. S. Ollila and G. Pabst, *Atomistic resolution structure and dynamics of lipid bilayers in simulations and experiments* (2016), in Press, URL http://dx.doi.org/10.1016/j.bbamem.2016.01.019.

[33] M. Hong, K. Schmidt-Rohr, and A. Pines, Journal of the American Chemical Society **117**, 3310 (1995).

[34] M. Hong, K. Schmidt-Rohr, and D. Nanz, Biophysical Journal **69**, 1939 (1995).

[35] J. D. Gross, D. E. Warschawski, and R. G. Griffin, Journal of the American Chemical Society **119**, 796 (1997).

[36] A. Botan, F. Favela-Rosales, P. F. J. Fuchs, M. Javanainen, M. Kandu, W. Kulig, A. Lamberg, C. Loison, A. Lyubartsev, M. S. Miettinen, et al., The Journal of Physical Chemistry B **119**, 15075 (2015).

[37] C. Altenbach and J. Seelig, Biochim. Biophys. Acta **818**, 410 (1985).

[38] P. M. Macdonald and J. Seelig, Biochemistry **26**, 1231 (1987).

[39] M. Roux and M. Bloom, Biochemistry **29**, 7077 (1990).

[40] G. Beschiaschvili and J. Seelig, Biochimica et Biophysica Acta (BBA) - Biomembranes **1061**, 78 (1991).

[41] F. M. Marassi and P. M. Macdonald, Biochemistry **31**, 10031 (1992).

[42] J. R. Rydall and P. M. Macdonald, Biochemistry **31**, 1092 (1992).

[43] J. Seelig, Cell biology international reports **14**, 353360 (1990), URL http://dx.doi.org/10.1016/0309-1651(90)91204-H.

[44] W. Zhao, A. A. Gurtovenko, I. Vattulainen, and M. Karttunen, The Journal of Physical Chemistry B **116**, 269 (2012).

[45] M. S. Miettinen, A. A. Gurtovenko, I. Vattulainen, and M. Karttunen, The Journal of Physical Chemistry B **113**, 9226 (2009).

[46] C. M. Franzin, P. M. Macdonald, A. Polozova, and F. M. Winnik, Biochimica et Biophysica Acta (BBA) - Biomembranes **1415**, 219 (1998).

[47] S. Ollila, M. T. Hyvönen, and I. Vattulainen, J. Phys. Chem. B **111**, 3139 (2007).

[48] O. H. S. Ollila, T. Ferreira, and D. Topgaard (2014), URL {http://dx.doi.org/10.5281/zenodo.13279}.

[49] T. P. Straatsma and H. J. C. Berendsen, The Journal of Chemical Physics **89** (1988).

[50] O. O. H. Samuli, *MD simulation trajectory and related files for POPC bilayer with 340mM NaCl (Berger model delivered by Tieleman, ffgmx ions, Gromacs 4.5)* (2015), URL http://dx.doi.org/10.5281/zenodo.32144.

[51] O. O. H. Samuli, *MD simulation trajectory and related files for POPC bilayer with 340mM CaCl_2 (Berger model delivered by Tieleman, ffgmx ions, Gromacs 4.5)* (2015), URL http://dx.doi.org/10.5281/zenodo.32173.

[52] S.-J. Marrink, O. Berger, P. Tieleman, and F. Jähnig, Biophysical Journal **74**, 931 (1998).

[53] J. Määttä (2015), URL {http://dx.doi.org/10.5281/zenodo.13934}.

[54] J. Mtt, *Dppc_berger_nacl* (2015), URL http://dx.doi.org/10.5281/zenodo.16319.

[55] J. Määttä, *Dppc_berger_nacl_1mol* (2015), URL http://dx.doi.org/10.5281/zenodo.17210.

[56] D. P. Tieleman, J. L. MacCallum, W. L. Ash, C. Kandt, Z. Xu, and L. Monticelli, J. Phys. Condens. Matter **18**, S1221 (2006).

[57] J. Määttä, *Dppc_berger_opls06* (2015), URL http://dx.doi.org/10.5281/zenodo.17237.

[58] J. Åqvist, The Journal of Physical Chemistry **94**, 8021 (1990).

[59] J. Määttä, *Dppc_berger_opls06_nacl* (2015), URL http://dx.doi.org/10.5281/zenodo.16484.

[60] J. Määttä, *Dppc_berger_opls06_nacl_1mol* (2016), URL http://dx.doi.org/10.5281/zenodo.46152.

[61] J. B. Klauda, R. M. Venable, J. A. Freites, J. W. O'Connor, D. J. Tobias, C. Mondragon-Ramirez, I. Vorobyov, A. D. M. Jr, and R. W. Pastor, J. Phys. Chem. B **114**, 7830 (2010).

[62] O. O. H. Samuli and M. Miettinen (2015), URL {http://dx.doi.org/10.5281/zenodo.13944}.

[63] R. M. Venable, Y. Luo, K. Gawrisch, B. Roux, and R. W. Pastor, The Journal of Physical Chemistry B **117**, 10183 (2013).

[64] S. Ollila, *MD simulation trajectory and related files for POPC bilayer with 350mM NaCl (CHARMM36, Gromacs 4.5)* (2015), URL http://dx.doi.org/10.5281/zenodo.32496.

[65] S. Ollila, *MD simulation trajectory and related files for POPC bilayer with 690mM NaCl (CHARMM36, Gromacs 4.5)* (2015), URL http://dx.doi.org/10.5281/zenodo.32497.

[66] S. Ollila, *MD simulation trajectory and related files for POPC bilayer with 950mM NaCl (CHARMM36, Gromacs 4.5)* (2015), URL http://dx.doi.org/10.5281/zenodo.32498.

[67] G. Mykhailo and O. O. H. Samuli, *Popc_charmm36_cacl2_035mol* (2015), URL http://dx.doi.org/10.5281/zenodo.35159.

[68] M. Javanainen, *POPC @ 310K, 450 mM of CaCl_2. Charmm36 with default Charmm ions* (2016), URL http://dx.doi.org/10.5281/zenodo.51185.

[69] G. Mykhailo and O. O. H. Samuli, *Popc_charmm36_cacl2_067mol* (2015), URL http://dx.doi.org/10.5281/zenodo.35160.

[70] G. Mykhailo and O. O. H. Samuli, *Popc_charmm36_cacl2_1mol* (2015), URL http://dx.doi.org/10.5281/zenodo.35156.

[71] J. Yoo, J. Wilson, and A. Aksimentiev, Biopolymers (2016).

[72] A. Maciejewski, M. Pasenkiewicz-Gierula, O. Cramariuc, I. Vattulainen, and T. Rog, The Journal of Physical Chemistry B **118**, 4571 (2014).

[73] M. Javanainen (2014), URL {http://dx.doi.org/10.5281/zenodo.13498}.

[74] M. Javanainen, *POPC @ 310K, varying amounts of NaCl. Model by Maciejewski and Rog* (2015), URL http://dx.doi.org/10.5281/zenodo.14976.

[75] O. H. S. Ollila, J. Mtt, and L. Monticelli, *MD simulation trajectory for POPC bilayer (Orange, Gromacs 4.5.)* (2015), URL http://dx.doi.org/10.5281/zenodo.34488.

[76] O. H. S. Ollila, J. Mtt, and L. Monticelli, *MD simulation trajectory for POPC bilayer with 140mM NaCl (Orange, Gromacs 4.5.)* (2015), URL http://dx.doi.org/10.5281/zenodo.34491.

[77] O. H. S. Ollila, J. Mtt, and L. Monticelli, *MD simulation trajectory for POPC bilayer with 510mM NaCl (Orange, Gromacs 4.5.)* (2015), URL http://dx.doi.org/10.5281/zenodo.34490.

[78] S. Ollila, J. Mtt, and L. Monticelli, *MD simulation trajectory for POPC bilayer with 1000mM NaCl (Orange, Gromacs 4.5.)* (2015), URL http://dx.doi.org/10.5281/zenodo.34497.

[79] O. H. S. Ollila, J. Mtt, and L. Monticelli, *MD simulation trajectory for POPC bilayer with 510mM CaCl_2 (Orange, Gromacs 4.5.)* (2015), URL http://dx.doi.org/10.5281/zenodo.34498.

[80] J. P. M. Jämbeck and A. P. Lyubartsev, The Journal of Physical Chemistry B **116**, 3164 (2012).

[81] J. Määttä (2014), URL {http://dx.doi.org/10.5281/zenodo.13287}.

[82] D. Beglov and B. Roux, The Journal of Chemical Physics **100** (1994).

[83] B. Roux, Biophysical Journal **71**, 3177 (1996), ISSN 0006-3495, URL http://www.sciencedirect.com/science/article/pii/S0006349596795115.

[84] J. P. M. Jämbeck and A. P. Lyubartsev, Journal of Chemical Theory and Computation **8**, 2938 (2012).

[85] M. Javanainen, *Popc @ 310k, slipids force field.* (2015), dOI: 10.5281/zenodo.13887.

[86] D. E. Smith and L. X. Dang, The Journal of Chemical Physics **100** (1994).

[87] M. Javanainen, *POPC @ 310K, 130 mM of NaCl. Slipids with ions by Smith & Dang* (2015), URL http://dx.doi.org/10.5281/zenodo.35275.

[88] M. Javanainen, *POPC @ 310K, 450 mM of CaCl_2. Slipids with default Amber ions* (2016), URL http://dx.doi.org/10.5281/zenodo.51182.

[89] C. J. Dickson, B. D. Madej, . A. Skjevik, R. M. Betz, K. Teigen, I. R. Gould, and R. C. Walker, Journal of Chemical Theory and Computation **10**, 865 (2014).

[90] M. Girych and O. H. S. Ollila, *Popc_amber_lipid14_verlet* (2015), URL http://dx.doi.org/10.5281/zenodo.30898.

[91] M. Girych and O. H. S. Ollila, *Popc_amber_lipid14_nacl_015mol* (2015), URL http://dx.doi.org/10.5281/zenodo.30891.

[92] M. Girych and O. H. S. Ollila, *Popc_amber_lipid14_nacl_1mol* (2015), URL http://dx.doi.org/10.5281/zenodo.30865.

[93] G. Mykhailo and O. O. H. Samuli, *Popc_amber_lipid14_cacl2_035mol* (2015), URL http://dx.doi.org/10.5281/zenodo.34415.

[94] G. Mykhailo and O. O. H. Samuli, *Popc_amber_lipid14_cacl2_1mol* (2015), URL http://dx.doi.org/10.5281/zenodo.35074.

[95] J. P. Ulmschneider and M. B. Ulmschneider, Journal of Chemical Theory and Computation **5**, 1803 (2009).

[96] M. Girych and O. H. S. Ollila, *Popc_ulmschneider_opls_verlet_group* (2015), URL http://dx.doi.org/10.5281/zenodo.30904.

[97] M. Girych and O. H. S. Ollila, *Popc_ulmschneider_opls_nacl_015mol* (2015), URL http://dx.doi.org/10.5281/zenodo.30892.

[98] M. Girych and O. H. S. Ollila, *Popc_ulmschneider_opls_nacl_1mol* (2015), URL http://dx.doi.org/10.5281/zenodo.30894.

[99] H. Hauser, M. C. Phillips, B. Levine, and R. Williams, Nature **261**, 390 (1976).

[100] H. Hauser, W. Guyer, B. Levine, P. Skrabal, and R. Williams, Biochimica et Biophysica Acta (BBA) - Biomembranes **508**, 450 (1978), ISSN 0005-2736, URL http://www.sciencedirect.com/science/article/pii/0005273678900913.

[101] L. Herbette, C. Napolitano, and R. McDaniel, Biophysical Journal **46**, 677 (1984).

[102] B. Hess, C. Holm, and N. van der Vegt, The Journal of Chemical Physics **124** (2006).

[103] A. A. Chen, , and R. V. Pappu, The Journal of Physical Chemistry B **111**, 11884 (2007).

[104] M. M. Reif, M. Winger, and C. Oostenbrink, Journal of Chemical Theory and Computation **9**, 1247 (2013), pMID: 23418406, http://dx.doi.org/10.1021/ct300874c, URL http://dx.doi.org/10.1021/ct300874c.

[105] I. Leontyev and A. Stuchebrukhov, Phys. Chem. Chem. Phys. **13**, 2613 (2011).

[106] W. L. Jorgensen, D. S. Maxwell, and J. Tirado-Rives, Journal of the American Chemical Society **118**, 11225 (1996).

[107] M. Kohagen, P. E. Mason, and P. Jungwirth, The Journal of Physical Chemistry B **120**, 1454 (2016).

[108] M. Kohagen, P. E. Mason, and P. Jungwirth, The Journal of Physical Chemistry B **118**, 7902 (2014).

[109] A. Arkhipov, Y. Shan, R. Das, N. Endres, M. Eastwood, D. Wemmer, J. Kuriyan, and D. Shaw, Cell **152**, 557 (2013).

[110] K. Kaszuba, M. Grzybek, A. Orowski, R. Danne, T. Rg, K. Simons, . Coskun, and I. Vattulainen, Proceedings of the National Academy of Sciences **112**, 4334 (2015).

[111] M. S. Miettinen, *Molecular dynamics simulation trajectory of a fully hydrated DMPC lipid bilayer* (2013), URL http://dx.doi.org/10.5281/zenodo.51635.

[112] M. S. Miettinen, *Molecular dynamics simulation trajectory of a cationic lipid bilayer: 6/94 mol% DMTAP/DMPC* (2016), URL http://dx.doi.org/10.5281/zenodo.51639.

[113] M. S. Miettinen, *Molecular dynamics simulation trajectory of a cationic lipid bilayer: 50/50 mol% DMTAP/DMPC* (2016), URL http://dx.doi.org/10.5281/zenodo.51748.

[114] J. Määttä (2015), URL {http://dx.doi.org/10.5281/zenodo.16320}.

[115] J. Määttä, *Dppc_berger_nacl_1mol_scaled* (2015), URL http://dx.doi.org/10.5281/zenodo.17228.

[116] J. Määttä (2015), URL {http://dx.doi.org/10.5281/zenodo.16485}.

[117] J. Mtt, *Dppc_berger_opls06_nacl_1mol_scaled* (2015), URL http://dx.doi.org/10.5281/zenodo.17209.

[118] M. Javanainen, *POPC @ 310K, varying amounts of NaCl. Slipids with ECC-scaled ions* (2015), URL http://dx.doi.org/10.5281/zenodo.35193.

[119] M. Javanainen, *POPC @ 310K, 450 mM of CaCl_2. Charmm36 with ECC-scaled ions* (2016), URL http://dx.doi.org/10.5281/zenodo.45008.

[120] M. Javanainen, *POPC @ 310K, 450 mM of CaCl_2. Slipids with ECC-scaled ions* (2016), URL http://dx.doi.org/10.5281/zenodo.45007.

[121] D. van der Spoel, E. Lindahl, B. Hess, A. R. van Buuren, E. Apol, P. J. Meulenhoff, D. P. Tieleman, A. L. T. M. Sijbers, K. A. Feenstra, R. van Drunen, et al., *GROMACS user manual version 4.0* (2005), URL www.gromacs.org.

[122] O. H. S. Ollila and et al. (2015), URL https://github.com/NMRLipids/lipid_ionINTERACTION.

[123] T. M. Ferreira, F. Coreta-Gomes, O. H. S. Ollila, M. J. Moreno, W. L. C. Vaz, and D. Topgaard, Phys. Chem. Chem. Phys. **15**, 1976 (2013).

[124] O. Berger, O. Edholm, and F. Jähnig, Biophys. J. **72**, 2002 (1997).

[125] M. Bachar, P. Brunelle, D. P. Tieleman, and A. Rauk, J. Phys. Chem. B **108**, 7170 (2004).

[126] B. Hess, H. Bekker, H. J. C. Berendsen, and J. G. E. M. Fraaije, J. Comput. Chem. **18**, 1463 (1997).

[127] B. Hess, Journal of Chemical Theory and Computation **4**, 116 (2008).

[128] T. Darden, D. York, and L. Pedersen, The Journal of Chemical Physics **98** (1993).

[129] U. L. Essman, M. L. Perera, M. L. Berkowitz, T. Larden, H. Lee, and L. G. Pedersen, J. Chem. Phys. **103**, 8577 (1995).

[130] G. Bussi, D. Donadio, and M. Parrinello, The Journal of Chemical Physics **126** (2007).

[131] M. Parrinello and A. Rahman, J. Appl. Phys. **52**, 7182 (1981).

[132] S. Pronk, S. Pll, R. Schulz, P. Larsson, P. Bjelkmar, R. Apostolov, M. R. Shirts, J. C. Smith, P. M. Kasson, D. van der Spoel, et al., Bioinformatics **29**, 845 (2013).

[133] H. J. C. Berendsen, J. P. M. Postma, W. F. van Gunsteren, A. DiNola, and J. R. Haak, J. Chem. Phys. **81**, 3684 (1984).

[134] J. Lee, X. Cheng, J. M. Swails, M. S. Yeom, P. K. Eastman, J. A. Lemkul, S. Wei, J. Buckner, J. C. Jeong, Y. Qi, et al., Journal of Chemical Theory and Computation **0**, null (0).

[135] M. J. Abraham, T. Murtola, R. Schulz, S. Pll, J. C. Smith, B. Hess, and E. Lindahl, SoftwareX **12**, 19 (2015), ISSN 2352-7110, URL http://www.sciencedirect.com/science/article/pii/S2352711015000059.

[136] S. Nose, Mol. Phys. **52**, 255 (1984).

[137] W. G. Hoover, Phys. Rev. A **31**, 1695 (1985).

[138] S. Pll and B. Hess, Computer Physics Communications **184**, 2641 (2013), ISSN 0010-4655, URL http://www.sciencedirect.com/science/article/pii/S0010465513001975.

[139] L. Martínez, R. Andrade, E. G. Birgin, and J. M. Martínez, J. Comput. Chem. **30**, 2157 (2009).

[140] W. Humphrey, A. Dalke, and K. Schulten, Journal of Molecular Graphics **14**, 33 (1996).

[141] J. C. Phillips, R. Braun, W. Wang, J. Gumbart, E. Tajkhorshid, E. Villa, C. Chipot, R. D. Skeel, L. Kalé, and K. Schulten, J. Comput. Chem. **26**, 1781 (2005).

[142] M. Abraham, D. van der Spoel, E. Lindahl, B. Hess, and the GROMACS development team, *GROMACS user manual version 5.0.7* (2015), URL www.gromacs.org.

[143] W. L. Jorgensen, J. D. Madura, and C. J. Swenson, Journal of the American Chemical Society **106**, 6638 (1984).

[144] W. L. Jorgensen and J. Gao, The Journal of Physical Chemistry **90**, 2174 (1986).

[145] W. L. Jorgensen, The Journal of Physical Chemistry **90**, 1276 (1986).

[146] W. L. Jorgensen and J. Tirado-Rives, Journal of the American Chemical Society **110**, 1657 (1988).

[147] J. M. Briggs, T. B. Nguyen, and W. L. Jorgensen, The Journal of Physical Chemistry **95**, 3315 (1991).

[148] W. L. Jorgensen, J. Chandrasekhar, J. D. Madura, R. W. Impey, and M. L. Klein, The Journal of Chemical Physics **79** (1983).

[149] O. H. S. Ollila and M. Retegan, *Md simulation trajectory and related files for popc bilayer (lipid14, gromacs 4.5)* (2014), URL http://dx.doi.org/10.5281/zenodo.12767.

[150] J. Domaski, P. Stansfeld, M. Sansom, and O. Beckstein, The Journal of Membrane Biology **236**, 255 (2010), ISSN 0022-2631.